IEEE Access
Multidisciplinary ⋮ Rapid Review ⋮ Open Access Journal

Received October 13, 2020, accepted October 21, 2020, date of publication October 26, 2020, date of current version November 9, 2020.

Digital Object Identifier 10.1109/ACCESS.2020.3033884

Parameter Selection and Optimization of an Intelligent Ultrasonic-Assisted Grinding System for SiC Ceramics

CHENG-JIAN LIN[1,2], (Senior Member, IEEE), JYUN-YU JHANG[3], AND KUU-YOUNG YOUNG[3], (Senior Member, IEEE)

[1]Department of Computer Science and Information Engineering, National Chin-Yi University of Technology, Taichung 41170, Taiwan
[2]College of Intelligence, National Taichung University of Science and Technology, Taichung 40401, Taiwan
[3]Institute of Electrical and Control Engineering, National Chiao Tung University, Hsinchu 30010, Taiwan

Corresponding author: Cheng-Jian Lin (cjlin@ncut.edu.tw)

This work was supported by the Ministry of Science and Technology of the Republic of China, Taiwan, under Contract MOST 108-2218-E-005-021 and MOST 109-2634-F-009-031.

ABSTRACT Ceramic grinding processing technology continues to advance rapidly. Recent studies are increasingly adopting ultrasonic-assisted grinding (UAG) for obtaining improved surface quality and reduced surface roughness. Because different grinding parameters could lead to different machining quality, operators may find it difficult to select grinding parameters on the basis of the expected machining quality alone. In this article, an intelligent UAG system (IUAGS) that provides suitable grinding parameters for the operator is proposed. This IUAGS employs a proposed one-dimensional convolutional neuro-fuzzy network (1DCNFN) to establish a surface roughness prediction model, and then a particle swarm optimization algorithm is used to optimize the grinding parameters. The experimental results demonstrate that our proposed 1DCNFN has a lower mean absolute percentage error (MAPE) in surface roughness prediction than other methods do. Moreover, our IUAGS can provide appropriate UAG parameters on the basis of the specific requirements of the operator.

INDEX TERMS Intelligent ultrasonic-assisted grinding system, ultrasonic-assisted grinding, grinding processing, convolutional neural fuzzy network, particle swarm optimization.

I. INTRODUCTION

In recent years, silicon carbide (SiC) has been widely used in aviation, automobile, and semiconductor industries [1]–[3]. SiC is a next-generation semiconductor material with excellent wear resistance, favorable corrosion resistance, and high thermal conductivity. However, SiC is hard and brittle; thus, material removal from SiC can lead to problems such as surface breakage, tool wear, and poor surface roughness. Many scholars have recently adopted ultrasonic-assisted grinding (UAG) systems to process ceramic materials and found that introducing UAG can improve machining quality considerably. For instance, Ding *et al.* [4] compared UAG with conventional grinding and found that UAG afforded less fiber fracture and 12% reduction in surface roughness. Moreover, Cao *et al.* [5] designed an ultrasonic-assisted internal grinding (UAIG) technique for grinding SiC ceramics and compared it with the conventional internal grinding technique. The results indicated that UAIG improved cylindricity accuracy and reduced surface roughness by 84.9%. Uhlmann and Bruckhoff [6] also reported that the use of UAG in the machining of ceramic matrix composites is able to reduce process forces significantly and increase material removal rates; it also shortened machining time and reduced machining force and tool wear.

In the machining process, surface roughness and milling accuracy are regarded as product quality indicators. The use of machining parameters to predict machining quality can not only save time but also reduce incurred costs. Chen and Tang [7] developed a mathematical model for predicting surface roughness in UAG to discuss the effect of the ultrasonic vibration amplitude on surface roughness. The authors noted the maximum error of different ultrasonic vibration amplitudes to be <15%. However, the

The associate editor coordinating the review of this manuscript and approving it for publication was Shun-Feng Su.

aforementioned model required experts to design complex mathematical formulas and did not consider all aspects of the problem. Consequently, the data-driven approach combined with machine learning is becoming a preferred method for constructing predictive models. Wu and Lei [8] used a back-propagation neural network (BPNN) to construct a forecast model for predicting the surface roughness of S45C steel: The vibration signals forming the time domain and frequency domain filtered out through Pearson correlation analysis were extracted as features. The cutting parameters and vibration signal features were then selected as the BPNN input. Their results indicated that prediction accuracy can be improved using cutting parameters and vibration signal features. Singh *et al.* [9] compared the effectiveness of surface roughness prediction models by using a neural network (NN) and adaptive-network-based fuzzy inference system (ANFIS). ANFIS [10] combines the advantages of the fuzzy inference system (FIS) and NN. An FIS resembles the human reasoning mechanism, making it more flexible in network design, whereas an NN enables the modelling of the nonlinear mapping of relationships between inputs and outputs. Singh *et al.* [9] used the standard deviation, mean-square error (MSE), and root MSE (RMSE) to evaluate the NN and ANFIS precision and found that these evaluation indicators for ANFIS were superior to those for NN. Cheri *et al.* [11] established a fuzzy NN (FNN) to predict the surface roughness of the cold-rolled steel strip. Although most artificial NNs (ANNs) adopt the gradient descent method [12] to update network parameters, the gradient descent method may lead to the local-minimum problem. Liu *et al.* [13] constructed a high-speed grinding temperature prediction model by introducing a particle swarm optimization (PSO) algorithm [14] to optimize the NN parameters. Xu *et al.* [15] proposed a prediction model to estimate tool life; in the prediction models, PSO and differential evolution (DE) algorithms [16] were used to adjust the ANFIS parameters, and these models were named PSO-ANFIS and DE-ANFIS, respectively. The results indicated that both PSO-ANFIS and DE-ANFIS provided better tool life prediction performance than did conventional ANN.

Deep learning technology is developing in tandem with the rapid developments in the high-performance hardware accelerator and graphics processing unit technologies. Currently, deep learning is applied in various fields, such as computer vision, natural language processing, autonomous vehicle technology, and medical image analysis [17]–[20]. The most popular deep learning architecture is the convolutional neural network (CNN), composed of a convolutional layer, a pooling layer, and a fully connected layer. Lin *et al.* [21] employed one-dimensional CNN (1DCNN) to predict the surface roughness in the milling process. The authors applied a convolution filter to automatically extract vibration signal raw data and reported that their 1DCNN provided highly accurate predictions. Ambadekar and Choudhari [22] designed a prediction system to monitor the flank wear of the cutting tool: To classify the cutting tool into different flank wear classes, the authors used cutting tool images as the CNN input; their experimental results indicated that the prediction accuracy of CNN was 87.26% in the classifying tasks. Compared with machine learning, deep learning can extract features automatically and construct models without handcraft designing, thus providing excellent prediction and classification performance. However, deep learning requires a large amount of memory and computational resources for training the network parameters.

The combination of different parameters affects different machining quality. Providing appropriate parameters through machining quality can be considered an optimization problem. Chandrasekaran and Tamang [23] developed a surface roughness prediction model by using an ANN, with spindle speed, feed rate, and cut depth as inputs and surface roughness as the output. Subsequently, the authors obtained a combination of optimum parameters through the adoption of the PSO. Fé-Perdomo *et al.* [24] designed a decision-making system for selecting optimal parameters in the micromilling process. The authors used an ANN to establish the micromilling process prediction model, followed by the cross-entropy method, to optimize the multi-objective problem. Their experimental results demonstrated that the decision-making system provided a reliable optimal solution in the micromilling process. Notably, those aforementioned methods depend on the high-accuracy prediction model. If the accuracy of the prediction model is insufficient, the parameters optimized by the evolutionary algorithm cannot achieve the expected results.

In the past studies, most of the researchers used the UAG parameters to establish the surface roughness prediction model. They did not consider using surface roughness value which required by the operator to generate the UAG process parameters. In this article, an intelligent UAG system (IUAGS) is developed to provide a suitable parameter combination according to the requirements of the operator in the UAG process. This IUAGS adopts the techniques of the one-dimensional convolutional neuro-fuzzy network (1DCNFN) and PSO algorithm. The proposed 1DCNFN (a combination of a convolutional layer and a neural fuzzy network) plays the role of a surrogate surface roughness prediction model, whereas the PSO aids in obtaining the optimization parameters of the grinding process. Finally, the experimental results illustrate the efficiency of the proposed IUAGS.

II. DATA COLLECTION

A. EXPERIMENTAL SETUP

The computer numerical controlled machine tool (MV184C, QUASER, Taiwan) [25] equipped with HEIDENHAIN TNC640 was used to collect the UAG experiment data. Fig. 1 and Table 1 present a photograph and specifications of the machine, respectively. To improve the grinding quality, the ultrasonic tool holder BT-40 (Hantop Intelligence Tech, Taiwan) [26] was also used. Fig. 2 and Table 2 present a photograph and specifications of BT-40, respectively.

FIGURE 1. QUASER-MV184C.

TABLE 1. Specifications of QUASER-MV184C.

Travel X/Y/Z (mm)	1020/610/610
Table size (mm)	1200×600
Max spindle speed (rpm)	12000
Table load capacity (kg)	500

FIGURE 2. BT40.

TABLE 2. Specifications of BT40.

Runout	μm	<5
Operating Freq.	Hz	20k~32k
Max. spindle speed	rpm	24,000
Weight	kg	2
Automatic tool changer		Yes

SiC ceramics have many advantages, such as excellent chemical resistance, high strength, and low thermal expansion capacity. The disadvantages of SiC is to chip easily, poor manufacturability, and low mechanical shock tolerance. Thus, it is important for SiC to select appropriate processing parameters. In the UAG experiments, SiC ceramics were used as the experimental material. The mechanical properties of SiC ceramic used are listed in Table 3. Moreover, Fig. 3 and Table 4 present a schematic and specifications of the diamond grinding pin LHM-DIA-D6.0-T5-K5-#60 [27] used in the experiment.

TABLE 3. mechanical properties of SiC ceramic.

Density (gm/cc)	3.1
Flexural Strength (MPa)	550
Elastic Modulus (GPa)	410
Compressive Strength (MPa)	3900
Hardness (Kg/mm^2)	2800
Fracture Toughness (MPa•m$^{1/2}$)	4.6
Maximum Use Temperature ($^\circ$C)	1650

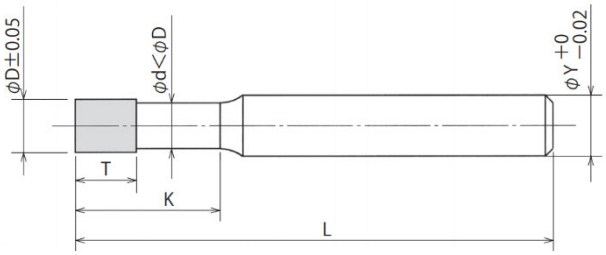

FIGURE 3. Diamond grinding pin.

TABLE 4. Specifications of the diamond grinding pin.

Head (mm)	Ø D	6.0
Width (mm)	T	5
Collar (mm)	K	5
Shank (mm)	Ø Y	8
Length (mm)	L	80

B. UAG PROCESSING PARAMETER DESIGN

The accuracy of a predictive model is critical to the effectiveness of its prediction. A good UAG experiment can not only collect experimental data in different grinding situations but also aid in constructing a high-precision prediction model. The main parameters that affect the CNC machining results are considered in this experiment, including cutting speed, feed rate, axial depth of cut, and radial depth of cut [28], [29]. In addition, different materials and ultrasonic power will also cause different surface roughness results [30], [31]. In this article, we focus on SiC materials and utilize five parameters mentioned above to design UAG experiments. The full factorial design method was used to collect the

TABLE 5. Parameters of UAG experiment.

Material	SiC
Cutting speed (mm/min)	75,90,105,120,135,150,165,180,195, 210,225
Feed rate (mm/min)	70,80,90,100,110,120,130,140, 150,160,170,180,190,200,210,220,23 0,240,250,260
Axial depth of cut (mm)	0.004,0.02
Radial depth of cut (mm)	5.5
Ultrasonic power (%)	0,10,30,60,100

UAG experiment data. As listed in Table 5, the UAG parameters include material, cutting speed, feed rate, cutting depth, cutting width, and ultrasonic power. The UAG experiments were performed a total of $11 \times 20 \times 2 \times 1 \times 5 = 2200$ times. Therefore, 2200 sets of data were collected, 80% of the data was used for predictive model training, and the remaining 20% was used for model testing.

C. SURFACE ROUGHNESS MEASUREMENT

After the UAG experiment, a 3D optical surface profiler (NewView^{TM} 8300, Zygo, USA) [32] was used to measure surface roughness of SiC. NewView^{TM} 8300 nondestructively provides a wide range of precise surface roughness measurements. Fig. 4 and Table 6 present a photograph and specifications of this profiler, respectively.

FIGURE 4. NewView^{TM} 8300.

III. IUAGS

This section introduces the proposed IUAGS. In UAG applications, the parameters for product quality with a specific requirement are usually determined on the basis of the experience of an expert. However, if an operator does not have any knowledge regarding the selection of the grinding parameters, starting a grinding process may be difficult. Thus, herein we propose an IUAGS that can assist an operator in grinding

TABLE 6. Specifications of NewView^{TM} 8300.

Travel X/Y (mm)	150/150
Tilt (°)	±4
Measurement Array	1024 x 1024
Field of View (mm)	0.04 to 16
Optical zoom (X)	1.0
Data Scan Speed (µm/sec)	96

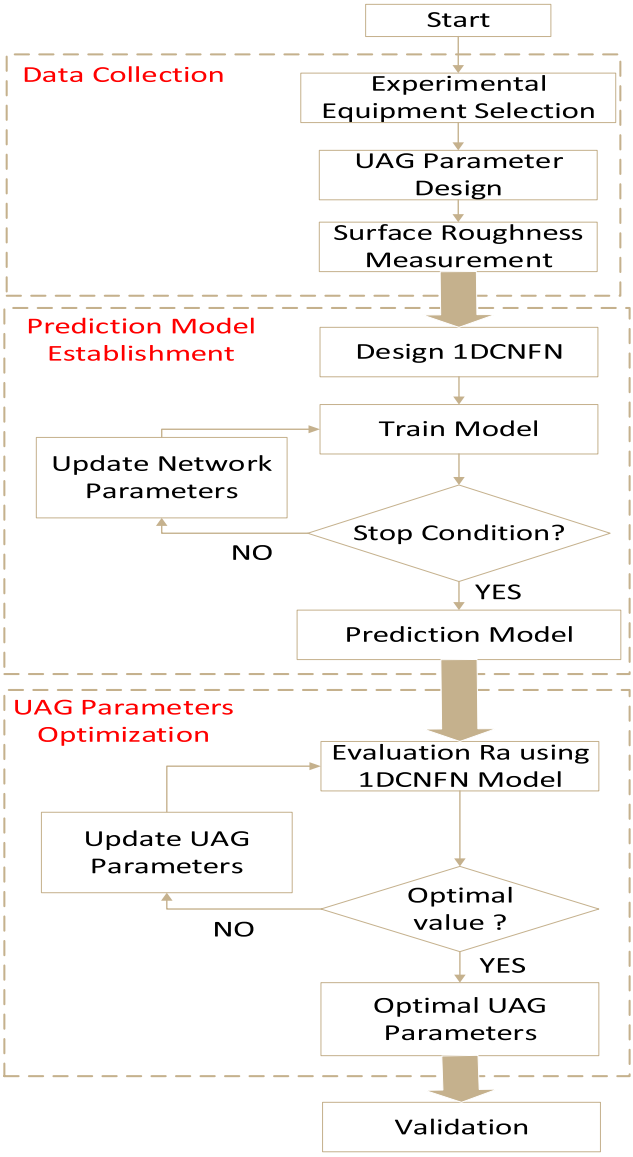

FIGURE 5. Flow of the proposed IUAGS.

parameter selection. Our IUAGS comprises three parts: data collection (as indicated in Section II), prediction model establishment, and UAG parameter optimization (Fig. 5). In brief,

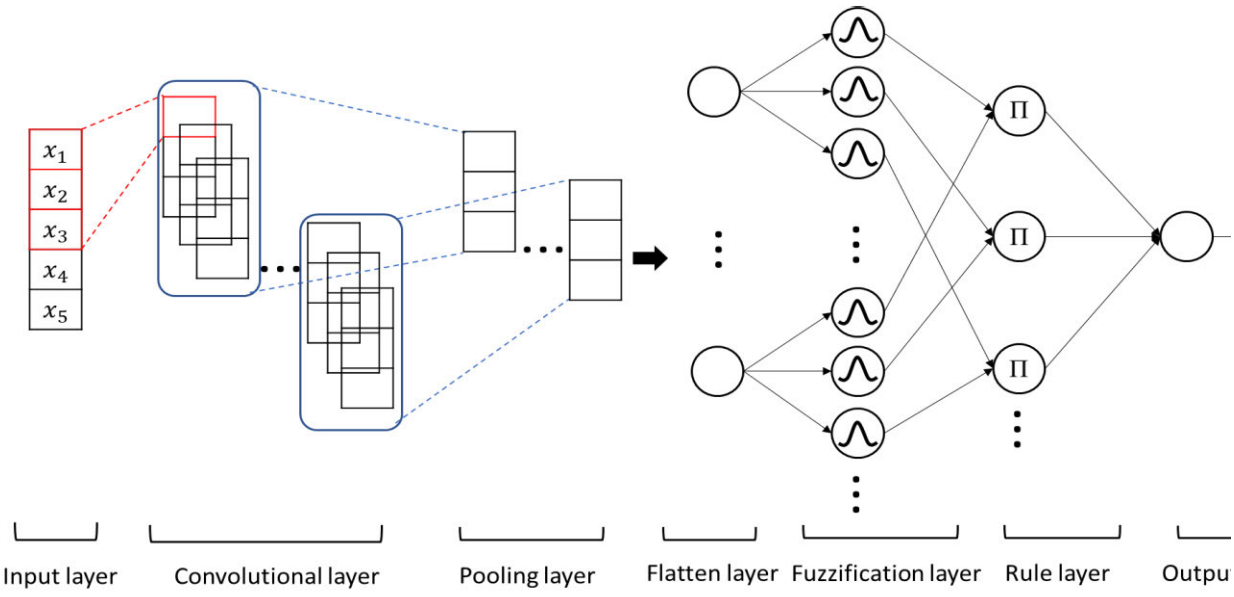

FIGURE 6. 1DCNFN structure.

after data collection, the prediction model is established using the proposed 1DCNFN, and the relationship between UAG parameters and surface roughness is obtained. Then, PSO is used to optimize the UAG parameters.

A. PROPOSED 1DCNFN FOR SURFACE ROUGHNESS PREDICTION

1) 1DCNFN STRUCTURE

Fig. 6 presents the structure of our 1DCNFN, which can be divided into input, convolutional, pooling, flatten, fuzzification, rule, and output layers. The convolutional layer aids feature extraction, whereas the prediction model is constructed on the neural fuzzy network.

The operation of each 1DCNFN layer is detailed as follows.

a: INPUT LAYER

The input X is i-nibble ($i = 1, \ldots, 5$) of one-dimensional raw data and passed to the next layer.

$$X = \{x_1, x_2, \ldots, x_i\} \tag{1}$$

b: CONVOLUTIONAL LAYER

The input is convolved with kernels with a restricted region of the visual field known as the receptive field to extract features in the convolutional layer. The operation of convolution is defined as

$$C_{pi} = \sum_{u=0}^{ks-1} x_{i+u} * k_{p,u} \tag{2}$$

where C denotes the convolution feature maps, p presents the number of convolution feature maps, $*$ denotes the convolution, ks is the convolution kernel size, $k \in \mathbb{R}$ is the convolution kernel (which randomly generates form the uniform distribution), and u is the column indices of the convolution kernel.

c: POOLING LAYER

Herein the channel max-pooling [33] is adopted to eliminate redundant information. The channel max-pooling compresses several feature maps to one by selecting the maximum value among the same locations. In contrast to the max-pooling operation, the channel max-pooling operation, which reduces the number of parameters by reducing the number of channels, does not change the width and the height of the feature map. The channel max-pooling operation is defined as

$$S_{mi} = \max_{1:G} C_{z,i}, \tag{3}$$

where S denotes the pooling feature maps, m is the number of pooling feature maps, G is the pooling kernel size, and z is the index of the convolution feature map, which is calculated as

$$z = (m-1)\, s + 1, \tag{4}$$

where s denotes the stride.

d: FLATTEN LAYER

The feature data that flatten into a one-dimensional vector is passed to the fuzzification layer. The operation of flattening is defined as

$$u_i = S_{mi}. \tag{5}$$

e: FUZZIFICATION LAYER

The fuzzy operation is calculated in this layer. The IF–THEN rule can be represented as

Rule$_j$: IF u_1 is A_{1j} and ... and u_n is A_{nj} THEN $y_j = w_j$, where A_{ij} represents the fuzzy sets, $i = 1, 2, \ldots K$, n is the

input numbers and $j = 1, 2, \ldots K$, r is the rule numbers, and w_j is a weight of zero-order Takagi–Sugeno–Kang type. The fuzzy set A_{ij}, which adopts a Gaussian membership function, is defined as

$$M_{ij} = exp\left\{-\frac{\left(u_i - m_{ij}\right)^2}{\sigma_{ij}^2}\right\}, \tag{6}$$

where m_{ij} and σ_{ij} are the mean and standard deviation of the fuzzy set A_{ij}. The advantage of using the Gaussian membership function is that it covers the whole input space to prevent the zero firing strength problem.

f: RULE LAYER

The firing strength of a fuzzy rule is calculated by the algebraic product operator as

$$R_j = \prod_{i=1}^{n} M_{ij}. \tag{7}$$

g: OUTPUT LAYER

The output y is calculated as

$$y = \sum_{j=1}^{r} R_j w_j. \tag{8}$$

2) PARAMETER LEARNING OF THE 1DCNFN

Herein the parameter learning method using the gradient descent algorithm for 1DCNFN is introduced. The objective to minimize the loss function is defined as

$$L = \frac{1}{2}\left(\hat{y} - y_d\right)^2 \tag{9}$$

where $\hat{y}$ and y_d are the model output and desired output of 1DCNFN. In parameter learning, the parameters containing w_j, m_{ij}, σ_{ij}, and $k_{p,u}$ update from the end to start. On the basis of the gradient descent algorithm, the updated parameters can be expressed as

$$w_j(t+1) = w_j(t) - \eta \Delta w_j \tag{10}$$

$$m_{ij}(t+1) = m_{ij}(t) - \eta \Delta m_{ij} \tag{11}$$

$$\sigma_{ij}(t+1) = \sigma_{ij}(t) - \eta \Delta \sigma_{ij} \tag{12}$$

$$k_{p,u}(t+1) = k_{p,u}(t) - \eta \Delta k_{p,u} \tag{13}$$

where $\eta \in (0, 1]$ represents the learning rate. The derivation of w_j can be expressed as follows:

$$\begin{aligned}\Delta w_j &= \frac{\partial L}{\partial w_j} = \frac{\partial L}{\partial \hat{y}}\frac{\partial \hat{y}}{\partial w_j} = \frac{\partial \frac{1}{2}\left(\hat{y} - y_d\right)^2}{\partial \hat{y}}\frac{\partial \sum_{j=1}^{r} R_j w_j}{\partial w_j} \\ &= (\hat{y} - y_d) R_j\end{aligned} \tag{14}$$

The derivation of m_{ij} and σ_{ij} can be expressed as follows:

$$\begin{aligned}\Delta m_{ij} &= \frac{\partial L}{\partial m_{ij}} = \frac{\partial L}{\partial M_{ij}}\frac{\partial M_{ij}}{\partial m_{ij}} = \frac{\partial L}{\partial R_j}\frac{\partial R_j}{\partial M_{ij}}\frac{\partial M_{ij}}{\partial m_{ij}} \\ &= \frac{\partial L}{\partial \hat{y}}\frac{\partial \hat{y}}{\partial R_j}\frac{\partial R_j}{\partial M_{ij}}\frac{\partial M_{ij}}{\partial m_{ij}} = (\hat{y} - y_d) w_j R_j \frac{2(u_i - m_{ij})}{\sigma_{ij}^2}\end{aligned} \tag{15}$$

$$\begin{aligned}\Delta \sigma_{ij} &= \frac{\partial L}{\partial \sigma_{ij}} = \frac{\partial L}{\partial M_{ij}}\frac{\partial M_{ij}}{\partial \sigma_{ij}} = \frac{\partial L}{\partial R_j}\frac{\partial R_j}{\partial M_{ij}}\frac{\partial M_{ij}}{\partial \sigma_{ij}} \\ &= \frac{\partial L}{\partial \hat{y}}\frac{\partial \hat{y}}{\partial R_j}\frac{\partial R_j}{\partial M_{ij}}\frac{\partial M_{ij}}{\partial \sigma_{ij}} = (\hat{y} - y_d) w_j R_j \frac{2\left(u_i - m_{ij}\right)^2}{\sigma_{ij}^3}\end{aligned} \tag{16}$$

Finally, the derivation of convolution kernel weights is expressed as follows:

$$\begin{aligned}\Delta k_{p,u} &= \frac{\partial L}{\partial k_{p,u}} = \frac{\partial L}{\partial C_{pi}}\frac{\partial C_{pi}}{\partial k_{p,u}} = \frac{\partial L}{\partial S_{mi}}\frac{\partial S_{mi}}{\partial C_{pi}}\frac{\partial C_{pi}}{\partial k_{p,u}} \\ &= \frac{\partial L}{\partial u_i}\frac{\partial u_i}{\partial S_{mi}}\frac{\partial S_{mi}}{\partial C_{pi}}\frac{\partial C_{pi}}{\partial k_{p,u}} = \frac{\partial L}{\partial M_{ij}}\frac{\partial M_{ij}}{\partial u_i}\frac{\partial u_i}{\partial S_{mi}}\frac{\partial S_{mi}}{\partial C_{pi}}\frac{\partial C_{pi}}{\partial k_{p,u}} \\ &= \frac{\partial L}{\partial R_j}\frac{\partial R_j}{\partial M_{ij}}\frac{\partial M_{ij}}{\partial u_i}\frac{\partial u_i}{\partial S_{mi}}\frac{\partial S_{mi}}{\partial C_{pi}}\frac{\partial C_{pi}}{\partial k_{p,u}} \\ &= \frac{\partial L}{\partial \hat{y}}\frac{\partial \hat{y}}{\partial R_j}\frac{\partial R_j}{\partial M_{ij}}\frac{\partial M_{ij}}{\partial u_i}\frac{\partial u_i}{\partial S_{mi}}\frac{\partial S_{mi}}{\partial C_{pi}}\frac{\partial C_{pi}}{\partial k_{p,u}} \\ &= (\hat{y} - y_d) w_j R_j \frac{-2(u_i - m_{ij})}{\sigma_{ij}^2}\frac{\partial S_{mi}}{\partial C_{pi}} x_{i+u}\end{aligned} \tag{17}$$

$$\frac{\partial S_{mi}}{\partial C_{pi}} = \begin{cases} 1, & C_{pi} \text{ is maximum value} \\ 0, & otherwise \end{cases} \tag{18}$$

B. UAG PARAMETER OPTIMIZATION

To establish our IUAGS, we combined 1DCNFN with a PSO algorithm. In general, a PSO algorithm is an evolutionary algorithm, inspired by the collective behavior of birds. Compared with other optimization algorithms, PSO requires fewer adjusting parameters, has global search ability, and provides fast convergence. Its mathematical model can be defined as

$$\begin{aligned}V_i(n+1) = \omega V_i(n) &+ C_1\varphi_1\left(P_{best} - X_i(n)\right) \\ &+ C_2\varphi_2\left(G_{best} - X_i(n)\right)\end{aligned} \tag{19}$$

and

$$X_i(n+1) = X_i(n) + V_i(n+1) \tag{20}$$

where $V_i(n)$ denotes the velocity for $X_i(n)$ particle, ω represents the inertia weight, C_1 and C_2 are the cognitive parameter and the social parameter, respectively, P_{best} is the personal best solution of the current particle, and G_{best} is the global best value of all particles; moreover, φ_1 and φ_2 are random numbers between [0, 1].

The fitness function $F(\cdot)$ of the PSO algorithm adopted in our IUAGS is defined as

$$F(\cdot) = \frac{1}{1 + (|T_{ra} - M_{ra}|)} \tag{21}$$

where T_{ra} represents the target surface roughness of the UAG process setting provided by the operator and M_{ra} is the predicted surface roughness provided by the prediction model. After the surface roughness prediction model using the proposed 1DCNFN is established, the goal of the fitness function of the PSO algorithm is to optimize the grinding parameters. If the fitness function value is higher and close to 1,

the approximate parameters of the target surface roughness can be obtained.

The steps of PSO for UAG parameter optimization are described as follows.

Step 1: Set the population size, maximum iteration, inertia weight ω, social coefficients C_1 and C_2.

Step 2: Encode UAG parameters as a particle and initialize randomly. Each particle represents a solution of UAG processing.

Step 3: Evaluate the fitness value of each particle by Eq.(21) and find out the personal best P_{best} and global best G_{best}.

Step 4: Update the velocity V_i and the position X_i of the particle according to Eqs.(19)-(20).

Step 5: Compute the fitness values. If the computed values are worse than previous particles, then abandon them. Otherwise, replace the previous particles.

Step 6: Repeat step 4-5 until the termination criterion is met (current iteration $\geq$ max iteration).

Step 7: Obtain the G_{best} as an optimal UAG parameter.

IV. EXPERIMENTAL RESULTS

In this section, we describe the experimental results in three parts: (i) analysis of variance (ANOVA) results for the relationship between the UAG parameters and surface roughness, (ii) surface roughness prediction results by adopting the proposed 1DCNFN and their comparison with different prediction models, and (iii) UAG processing results with optimized parameters on our IUAGS.

A. UAG PARAMETER ANALYSIS

To establish a high-precision prediction model, we used the full factorial design method for collecting the UAG experiment data. After data collection, we employed ANOVA, which can quantify the effect of various input factors affecting processing, to estimate the percentage contribution (P_c) of process factors on the UAG experiment data. The analyzed UAG factors included cutting speed (11 levels), feed rate (20 levels), axial cutting depth (2 levels), and ultrasonic power (5 levels). The P_c for each UAG factor was calculated as follows:

$$DOF = K_A - 1 \tag{22}$$

$$SS_A = \sum_{i=1}^{K_A} \left(\frac{A_i^2}{n_{A_i}} \right) - \frac{T^2}{N} \tag{23}$$

$$SS_T = \sum_{i=1}^{N} y_i^2 - \frac{T^2}{N} \tag{24}$$

$$SS_E = SS_T - (SS_A + SS_B + \ldots) \tag{25}$$

Here, DOF denotes degrees of freedom, SS_A presents the sum of squares for factor A, SS_T presents the total sum of squares, SS_E presents the error sum of squares, K_A is the number of levels for factor A, A_i is the summation of all observations of level i for factor A, n_{A_i} is the number of all observations at level i for factor A, T is the summation of all observations, N is the total number of experiments, and y_i is the observation of i.

$$MS_A = \frac{SS_A}{DF} \tag{26}$$

$$MS_E = \frac{SS_E}{DF} \tag{27}$$

$$F_A = \frac{MS_A}{MS_E} \tag{28}$$

$$P_c = \frac{SS_A}{SS_T} \times 100\% \tag{29}$$

Here, MS_A denotes the variance of each factor, MS_E is the MSE, F_A represents the F ratio of factor A, and P_c is the percentage of contribution for each factor. The higher the P_c, the more significant is the factor to the results. Table 7 presents the ANOVA results.

TABLE 7. Anova results for the UAG experiment.

Source	DF	SS	MS	F	PC (%)
Cutting speed	10	12.20	1.2198	95.18	3.57
Feed rate	19	210.92	11.1010	866.18	61.69
Axial depth of cut	1	11.31	11.3128	882.70	3.3
Ultrasonic power	4	79.72	19.9301	1555.09	23.32
Error	2165	27.75	0.0128	—	8.12
Total	2199	341.90	—	—	100

As displayed in Table 7, the most significant factors contributing to surface roughness were found to be feed rate (61.69%), followed by ultrasonic power (23.32%), whereas cutting speed (3.57%) and axial cut depth (3.31%) were found to be the least significant. On the other hand, the total contribution rate of main parameters reaches 80%, the insignificant parameters can be ignored. If the error of percent contribution (uncontrolled and unknown factors) is <50%, it can assume that no significant factor has been omitted in the experiment. In our UAG experiment, the error of percent contribution was 8.12%, indicating that no significant factor has been omitted.

B. SURFACE ROUGHNESS PREDICTION RESULTS

We next compared the proposed 1DCNFN with different models containing BPNN [8], ANFIS [10], FNN [11], and 1DCNN [21] to verify the prediction effectiveness. Here, the 1DCNN (used for comparison) has two convolutional layers, one pooling layer, and one fully connected layer; its architecture 1DCNN is detailed in Table 8. Of the 2200 sets of experiment data collected from the UAG experiment, 80% (1760) was denoted as training data and 20% (440) was denoted as testing data. Each model was trained through 1000 iterations, followed by the evaluation of its effectiveness by using evaluation functions. The performance of the testing data for each surface roughness prediction model is shown in Fig. 8: among all prediction model networks, the BPNN

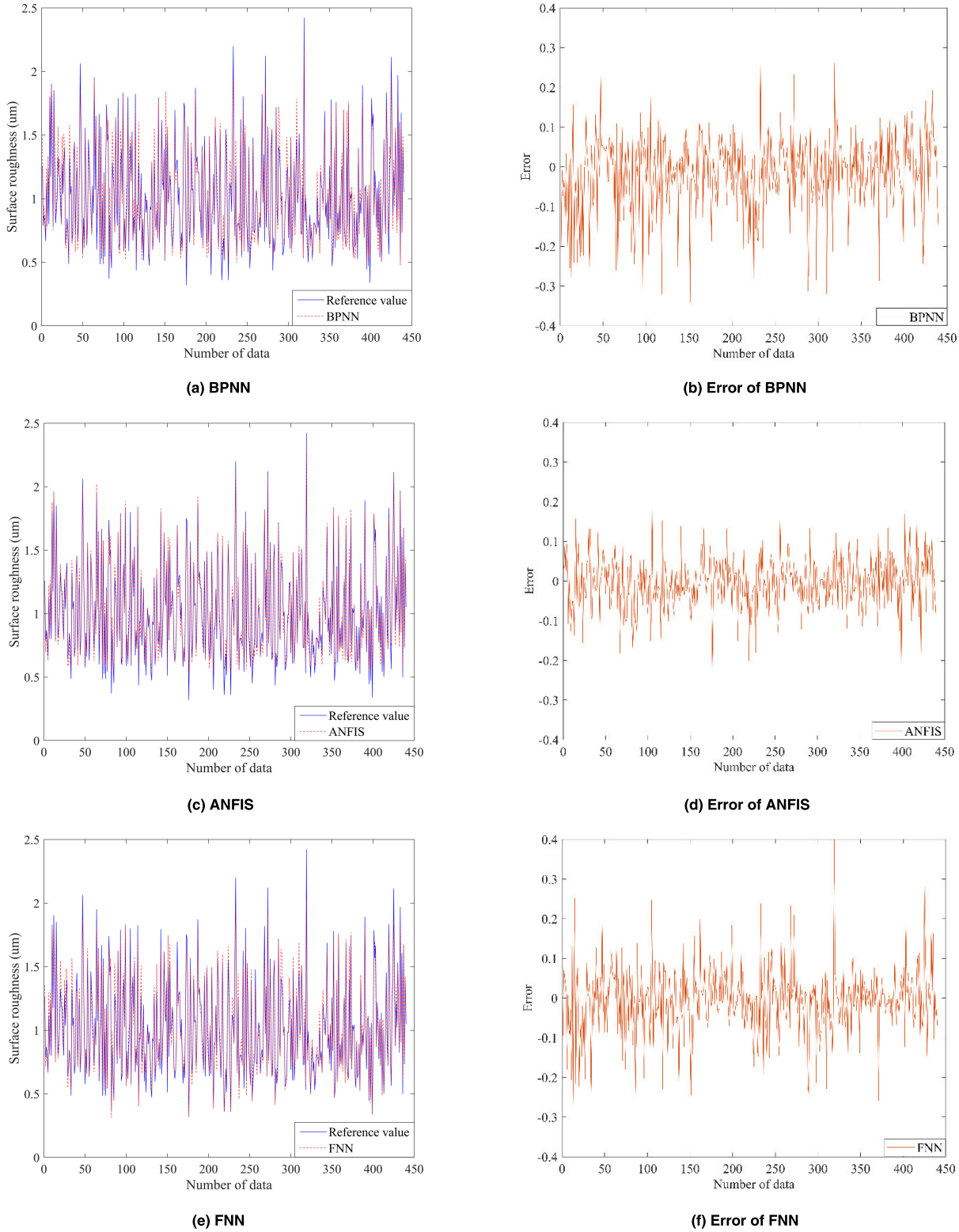

(a) BPNN

(b) Error of BPNN

(c) ANFIS

(d) Error of ANFIS

(e) FNN

(f) Error of FNN

FIGURE 7. Performance of testing data for each prediction model.

demonstrated the largest prediction error, followed by ANFIS and FNN, whereas the 1DCNN and 1DCNFN afforded the smallest prediction errors.

Moreover, we used different evaluation functions to evaluate the effectiveness of each model. These evaluation functions included MSE, RMSE, mean absolute error (MAE), and

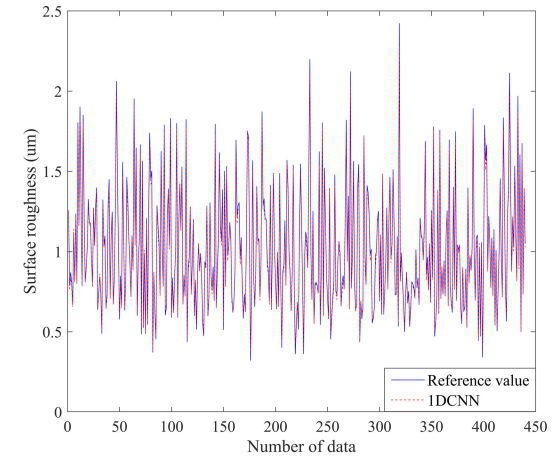

(g) 1DCNN

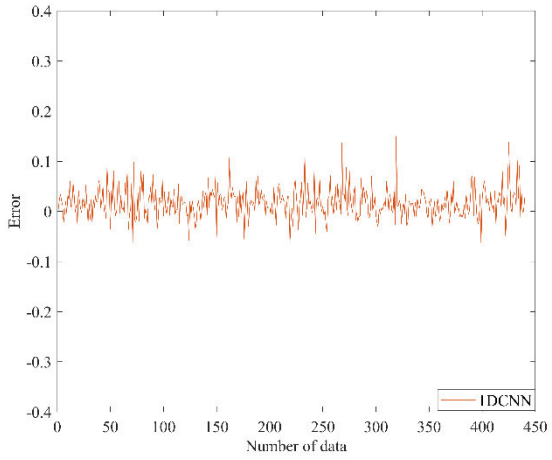

(h) Error of 1DCNN

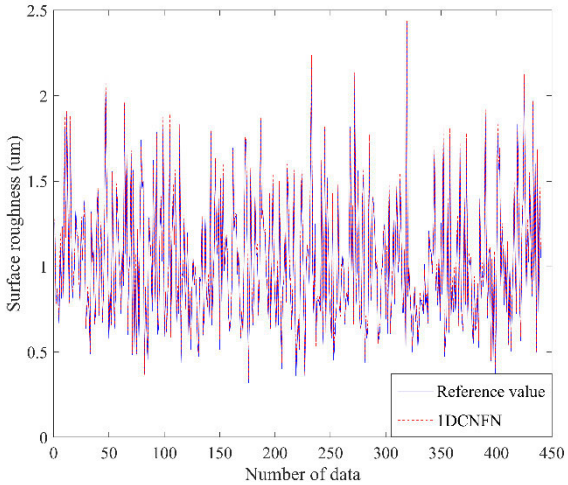

(i) 1DCNFN

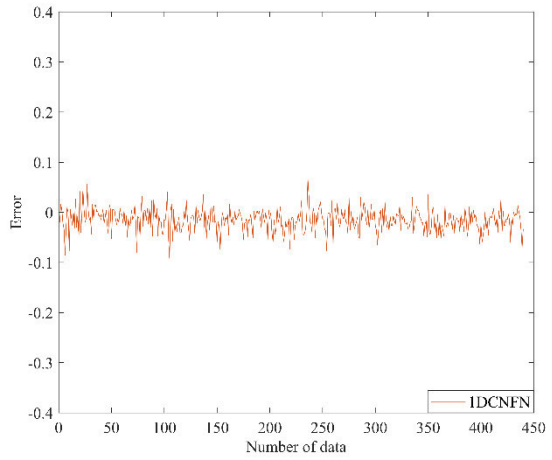

(j) Error of 1DCNFN

FIGURE 7. ***(Continued.)*** **Performance of testing data for each prediction model.**

TABLE 8. **1DCNN architecture.**

Layer	Parameter size
Input	1×5
Conv1 (size, channel)	1×3,20
Conv2 (size, channel)	1×3, 80
Max pooling (size)	1×3
Fully connected	1×32
Output	1

mean absolute percentage error (MAPE). These evaluation functions are defined as follows:

$$MSE = \frac{1}{n}\sum_{i=1}^{n}(\hat{y}_i - y_i)^2 \tag{30}$$

$$RMSE = \sqrt{\frac{1}{n}\sum_{i=1}^{n}(\hat{y}_i - y_i)^2} \tag{31}$$

$$MAE = \frac{1}{n}\sum_{i=1}^{n}\left|\hat{y}_i - y_i\right| \tag{32}$$

$$MAPE = \frac{100\%}{n}\sum_{i=1}^{n}\left|\frac{\hat{y}_i - y_i}{y_i}\right| \tag{33}$$

Here, $\hat{y}_i$ denotes the actual measured surface roughness value, y_i is the predicted value, and n presents the number of data. Different MAPE values indicate different prediction performance [34].

The levels of different prediction performances are listed in Table 9, and the detailed prediction results are summarized in Table 10. As presented in Table 10, the MAPE of all established prediction models was <10%, indicating that all the prediction models had high accuracy. Compared with other models, those with 1DCNN and the proposed 1DCNFN had lower MAPE (2.61% and 2.41%, respectively).

In this experiment, the total number of adjustable parameters of each prediction model were also compared in Table 11. As shown in Tables 10 and 11, BPNN, ANFIS, and FNN

TABLE 9. Prediction performance of MAPE.

MAPE	Performance
<10%	Highly accurate
10%-20%	Accurate
20%-50%	Reasonable
>50%	Not accurate

TABLE 10. Prediction performance of MAPE.

Indicator / Model	MSE	RMSE	MAE	MAPE
BPNN	0.0098	0.0994	0.0731	7.89%
ANFIS	0.0042	0.0648	0.0503	6.25%
FNN	0.0073	0.0858	0.0608	6.07%
1DCNN	0.0012	0.0347	0.0261	2.61%
1DCNFN	0.0007	0.0273	0.0214	2.41%

TABLE 11. Number of adjustable parameters of the prediction model.

Model	Number of Parameters
BPNN	112
ANFIS	104
FNN	176
1DCNN	10,145
1DCNFN	768

had fewer parameters (n < 200) but their MAPE was greater than 5%. Although the 1DCNN had a high prediction accuracy (MAPE < 5%), it contained more than 10,000 parameters. In contrast, the proposed 1DCNFN has less than 1000 parameters and is superior to other models in surface roughness prediction accuracy (i.e., it has a lower MAPE). In manufacturing, the computing resources of each equipment are precious. The proposed 1DCNFN can achieve the performance of traditional 1DCNN with fewer parameters and calculations without the need for expensive GPU hardware costs. Therefore, the proposed 1DCNFN can be easily implemented on embedded devices.

C. UAG PARAMETER OPTIMIZATION RESULTS

We applied the PSO algorithm to determine the optimization solution and provide operators with suitable UAG processing parameters. Table 12 lists the initial parameters of PSO, including the number of particles, the single inertia weight ω, acceleration constants C_1 and C_2, and number of iterations.

TABLE 12. Initial parameters of PSO.

Number of particles	Inertia weight (ω)	C_1	C_2	Iteration
30	0.5	2	2	500

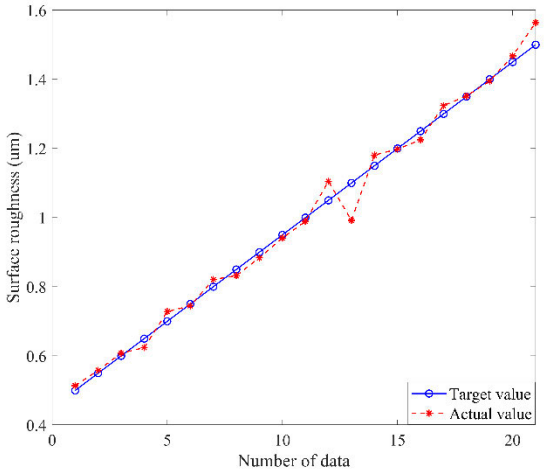

FIGURE 8. Experimental results of UAG processing.

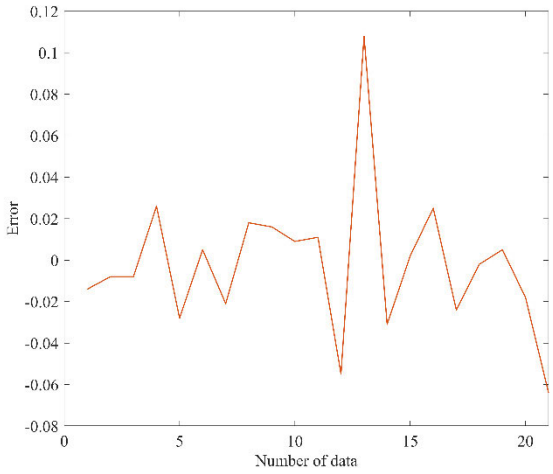

FIGURE 9. Error of UAG processing.

The UAG parameters were generated by using the proposed IUAGS according to the requirement of the operator. Then, UAG processing was performed using the generated parameters on the QUASER-MV184C machine tool. In this experiment, we set different target surface roughness values, ranging from 0.5 to 1.5 (um), for performance evaluation. The experimental results are illustrated in Figs. 8 and 9: the performance of UAG processing with 12th, 13th, and 21st parameters were not as satisfactory as expected. Table 13 provides the detailed experimental results of each UAG process: the 21 sets of parameters for UAG processing selected by our IUAGS had a low MAPE (2.43%). Taken together, these results indicated that the proposed IUAGS can

TABLE 13. Prediction performance of MAPE.

No.	Target Ra	Actual Ra	MSE	RMSE	MAE	MAPE
1	0.5	0.514				
2	0.55	0.558				
3	0.6	0.608				
4	0.65	0.624				
5	0.7	0.728				
6	0.75	0.745				
7	0.8	0.821				
8	0.85	0.832				
9	0.9	0.884				
10	0.95	0.941				
11	1	0.989	0.0011	0.0340	0.0237	2.43%
12	1.05	1.105				
13	1.1	0.992				
14	1.15	1.181				
15	1.2	1.198				
16	1.25	1.225				
17	1.3	1.324				
18	1.35	1.352				
19	1.4	1.395				
20	1.45	1.468				
21	1.5	1.564				

provide suitable parameters for UAG processing with high accuracy.

V. CONCLUSION

In UAG processing, grinding parameters have direct effects on the product quality, and an operator may not have the expertise of selecting suitable parameters. Herein we designed an IUAGS that can assist the operator in selecting suitable UAG processing parameters. Our IUAGS contains our newly proposed 1DCNFN for establishing the surface roughness prediction model; in this 1DCNFN, a convolutional layer and an FNN are combined to facilitate automatic feature extraction and increase prediction accuracy. To find the optimal combination of grinding parameters for expected surface roughness, the PSO algorithm is applied subsequently. Our experimental results demonstrated that the IUAGS can aid in selecting the most suitable UAG parameters on the basis of the quality requirements at high accuracy, as indicated by the low MAPE (2.43%).

REFERENCES

[1] J. Steibel, "Ceramic matrix composites taking flight at GE Aviation," *Amer. Ceram. Soc. Bull.*, vol. 98, pp. 30–33, Apr. 2019.

[2] K. Tatsumi, M. Inagaki, K. Kamei, T. Iizuka, H. Narimatsu, N. Sato, K. Shimizu, K. Ueda, A. Imakiire, M. Hikita, R. Kamimura, K. Sugiura, K. Tsuruta, and K. Toda, "Development of packaging technology for high temperature resistant SiC module of automobile application," in *Proc. IEEE 67th Electron. Compon. Technol. Conf. (ECTC)*, May 2017, pp. 1316–1321.

[3] S. Ji, Z. Zhang, and F. Wang, "Overview of high voltage sic power semiconductor devices: Development and application," *CES Trans. Electr. Mach. Syst.*, vol. 1, no. 3, pp. 254–264, Sep. 2017.

[4] K. Ding, Y. Fu, H. Su, F. Cui, Q. Li, W. Lei, and H. Xu, "Study on surface/subsurface breakage in ultrasonic assisted grinding of C/SiC composites," *Int. J. Adv. Manuf. Technol.*, vol. 91, nos. 9–12, pp. 3095–3105, Aug. 2017.

[5] J. Cao, Y. Wu, D. Lu, M. Fujimoto, and M. Nomura, "Fundamental machining characteristics of ultrasonic assisted internal grinding of SiC ceramics," *Mater. Manuf. Processes*, vol. 29, no. 5, pp. 557–563, May 2014.

[6] E. Uhlmann and J. Bruckhoff, "Interaction of tool and workpiece in ultrasonic-assisted grinding of high performance ceramics," *Procedia Manuf.*, vol. 33, pp. 762–769, 2019.

[7] H. Chen and J. Tang, "A model for prediction of surface roughness in ultrasonic-assisted grinding," *Int. J. Adv. Manuf. Technol.*, vol. 77, nos. 1–4, pp. 643–651, Mar. 2015.

[8] T. Y. Wu and K. W. Lei, "Prediction of surface roughness in milling process using vibration signal analysis and artificial neural network," *Int. J. Adv. Manuf. Technol.*, vol. 102, nos. 1–4, pp. 305–314, May 2019.

[9] N. K. Singh, Y. Singh, S. Kumar, and A. Sharma, "Predictive analysis of surface roughness in EDM using semi-empirical, ANN and ANFIS techniques: A comparative study," *Mater. Today, Proc.*, vol. 25, pp. 735–741, 2020.

[10] D. Karaboga and E. Kaya, "Adaptive network based fuzzy inference system (ANFIS) training approaches: A comprehensive survey," *Artif. Intell. Rev.*, vol. 52, no. 4, pp. 2263–2293, Dec. 2019.

[11] S.-H. Cheri, J.-G. Wang, and T.-Q. Gu, "An online intelligent control method for surface roughness of cold-rolled strip steel," in *Proc. 37th Chin. Control Conf. (CCC)*, Jul. 2018, pp. 8330–8335.

[12] Y. Chen and D. Miao, "Granular regression with a gradient descent method," *Inf. Sci.*, vol. 537, pp. 246–260, Oct. 2020.

[13] C. Liu, W. Ding, Z. Li, and C. Yang, "Prediction of high-speed grinding temperature of titanium matrix composites using BP neural network based on PSO algorithm," *Int. J. Adv. Manuf. Technol.*, vol. 89, nos. 5–8, pp. 2277–2285, Mar. 2017.

[14] D. Wang, D. Tan, and L. Liu, "Particle swarm optimization algorithm: An overview," *Soft Comput.*, vol. 22, no. 2, pp. 387–408, Jan. 2018.

[15] L. Xu, C. Huang, R. Su, H. Zhu, H. Liu, Y. Liu, C. Li, and J. Wang, "Estimation of tool life and cutting burr in high speed milling of the compacted graphite iron by DE based adaptive neuro-fuzzy inference system," *Mech. Sci.*, vol. 10, no. 1, pp. 243–254, Jun. 2019.

[16] K. R. Opara and J. Arabas, "Differential evolution: A survey of theoretical analyses," *Swarm Evol. Comput.*, vol. 44, pp. 546–558, Feb. 2019.

[17] A. Voulodimos, N. Doulamis, A. Doulamis, and E. Protopapadakis, "Deep learning for computer vision: A brief review," *Comput. Intell. Neurosci.*, vol. 2018, Feb. 2018, Art. no. 7068349.

[18] T. Young, D. Hazarika, S. Poria, and E. Cambria, "Recent trends in deep learning based natural language processing," *IEEE Comput. Intell. Mag.*, vol. 13, no. 3, pp. 55–75, Aug. 2018.

[19] A. Miglani and N. Kumar, "Deep learning models for traffic flow prediction in autonomous vehicles: A review, solutions, and challenges," *Veh. Commun.*, vol. 20, Dec. 2019, Art. no. 100184.

[20] G. Litjens, T. Kooi, B. E. Bejnordi, A. A. A. Setio, F. Ciompi, M. Ghafoorian, J. A. W. M. van der Laak, B. van Ginneken, and C. I. Sánchez, "A survey on deep learning in medical image analysis," *Med. Image Anal.*, vol. 42, pp. 60–88, Dec. 2017.

[21] W.-J. Lin, S.-H. Lo, H.-T. Young, and C.-L. Hung, "Evaluation of deep learning neural networks for surface roughness prediction using vibration signal analysis," *Appl. Sci.*, vol. 9, no. 7, p. 1462, Apr. 2019.

[22] P. K. Ambadekar and C. M. Choudhari, "CNN based tool monitoring system to predict life of cutting tool," *Social Netw. Appl. Sci.*, vol. 2, no. 5, p. 860, May 2020.

[23] M. Chandrasekaran and S. Tamang, "ANN–PSO integrated optimization methodology for intelligent control of MMC machining," *J. Inst. Eng. C*, vol. 98, no. 4, pp. 395–401, Aug. 2017.

[24] I. la Fe-Perdomo, G. Beruvides, R. Quiza, R. Haber, and M. Rivas, "Automatic selection of optimal parameters based on simple soft-computing methods: A case study of micromilling processes," *IEEE Trans. Ind. Informat.*, vol. 15, no. 2, pp. 800–811, Feb. 2019.

[25] *MV184 Specification*, QUASER, Taichung City, Taiwan, 2019.

[26] *Product BT Series*, Hantop Intell. Tech., Taichung City, Taiwan, 2018.

[27] *LHMS Series*, RESMOTOOL, Higashiomi, Japan, 2013.

[28] Y. Yao, Y. Li, Q. Chen, and S. Wang, "Optimize CNC milling parameters on-line," in *Proc. Int. Conf. Measuring Technol. Mechatronics Autom.*, vol. 2, Mar. 2010, pp. 856–859.

[29] M. V. Vardhan, G. Sankaraiah, M. Yohan, and H. J. Rao, "Optimization of parameters in CNC milling of P20 steel using response surface methodology and taguchi method," *Mater. Today, Proc.*, vol. 4, no. 8, pp. 9163–9169, 2017.

[30] M. H. M. Ghazali, A. Z. A. Mazlan, L. M. Wei, C. T. Tying, T. S. Sze, and N. I. M. Jamil, "Effect of machining parameters on the surface roughness for different type of materials," *IOP Conf., Mater. Sci. Eng.*, vol. 530, Jul. 2019, Art. no. 012008.
[31] S. J. Wang, S. To, and C. F. Cheung, "Effect of workpiece material on surface roughness in ultraprecision raster milling," *Mater. Manuf. Processes*, vol. 27, no. 10, pp. 1022–1028, Oct. 2012.
[32] *NewView Product Manuals*, ZYGO, Berwyn, PA, USA, 2017.
[33] Z. Ma, D. Chang, J. Xie, Y. Ding, S. Wen, X. Li, Z. Si, and J. Guo, "Fine-grained vehicle classification with channel max pooling modified CNNs," *IEEE Trans. Veh. Technol.*, vol. 68, no. 4, pp. 3224–3233, Apr. 2019.
[34] C. D. Lewis, *Industrial and Business Forecasting Methods: A Practical Guide to Exponential Smoothing and Curve Fitting*. London, U.K.: Butterworth, 1982.

CHENG-JIAN LIN (Senior Member, IEEE) received the B.S. degree in electrical engineering from the Tatung Institute of Technology, Taipei, Taiwan, R.O.C., in 1986, and the M.S. and Ph.D. degrees in electrical and control engineering from the National Chiao-Tung University, Taiwan, in 1991 and 1996, respectively. He is currently a Chair Professor of the Computer Science and Information Engineering Department, National Chin-Yi University of Technology, Taichung, Taiwan, and the Dean of Intelligence College, National Taichung University of Science and Technology, Taichung. His current research interests include machine learning, pattern recognition, intelligent control, image processing, intelligent manufacturing, and evolutionary robot.

JYUN-YU JHANG received the B.S. and M.S. degrees from the Department of Computer Science and Information Engineering, National Chin-Yi University of Technology, Taichung, Taiwan, in 2015. He is currently pursuing the Ph.D. degree with the Institute of Electrical and Control Engineering, National Chiao Tung University, Hsinchu, Taiwan. His current research interests include fuzzy logic theory, type-2 neural fuzzy systems, evolutionary computation, machine learning, computer vision, and application.

KUU-YOUNG YOUNG (Senior Member, IEEE) received the B.S. degree in electrical engineering from National Taiwan University, Taiwan, in 1983, and the M.S. and Ph.D. degrees in electrical engineering from Northwestern University, Evanston, IL, USA, in 1987 and 1990, respectively. He is currently a Professor with the Electrical Engineering Department, National Chiao-Tung University, Hsinchu, Taiwan. His current research interests include intelligent control, image processing, and robotic control.